Analysis of an alternative to the H–atom abstraction mechanism in methane C–H bond activation by nonheme iron(IV)–oxo oxidants

ARTICLE *in* DALTON TRANSACTIONS · JUNE 2013

Impact Factor: 4.2 · DOI: 10.1039/c3dt50866h · Source: PubMed

4 AUTHORS, INCLUDING:

Jia Guan
Texas A&M University
10 PUBLICATIONS **58** CITATIONS
SEE PROFILE

Xuri Huang
Jilin University
43 PUBLICATIONS **167** CITATIONS
SEE PROFILE

Dalton Transactions

RSC Publishing

PAPER

View Article Online
View Journal | View Issue

Cite this: *Dalton Trans.*, 2013, **42**, 10260

Analysis of an alternative to the H-atom abstraction mechanism in methane C–H bond activation by nonheme iron(IV)-oxo oxidants†

Hao Tang, Jia Guan, Huiling Liu* and Xuri Huang*

Received 1st April 2013,
Accepted 9th May 2013

DOI: 10.1039/c3dt50866h

www.rsc.org/dalton

The triplet δ-mechanism different from the previously reported ones, *i.e.*, the π-channel with the unoccupied $\pi^*_{xz/yz}$ (FeO) orbital and the σ-channel involving the unoccupied α-spin Fe-σ^*_{z2} orbital, has been theoretically described for the methane hydroxylation by $[Fe^{IV} = O(TMC)(SR)]^+$ and its derivative $[Fe^{IV} = O(TMC)(OH)]^+$ complex for the first time, and we have undertaken a detailed DFT study on the nature of this state by probing its geometry, electronic property and reactivity in comparison to all other possibilities. DFT calculations indicate that the electron transfer for the $^3\delta$-channel from the σ_{C-H} orbital of the substrate to the final acceptor σ^*_{x2-y2} orbital of the catalyst occurs through a complex mechanism, which is initiated by the original α-spin electron transfer from the π* orbital of the catalyst to the σ^*_{x2-y2} orbital, where the α-spin electron from the σ_{C-H} orbital of the substrate shifts to the just empty α-spin π* orbital of the catalyst *via* the O-$p_{x/y}$ based $\pi^*_{xz/yz}$-orbital concomitantly. It is also found that the electron-donating ability of the axial ligand could influence the reaction channels, evident by the distinction that the electron-deficient F^- and $CF_3CO_2^-$ ligands react *via* the $^3\sigma$-channel, whereas the electron-rich SR^- and OH^- ligands proceed by the $^3\delta$-channel. With respect to reactivity, the $^3\delta$-pathway has a comparable barrier to the $^3\pi$ and $^5\pi$-pathways, which may offer a new approach for the specific control of C–H bond activation by the iron(IV)-oxo species.

Introduction

High-valence iron(IV)-oxo species have attracted widespread attention recently, since the enzymatic heme intermediates and synthetic nonheme compounds have been proposed to be highly active oxidants in C–H bond activation reactions.[1–6] Whereas the enzymatic complexes are generally characterized by high-spin quintet ($S = 2$) ground states, a wide range of synthetic variants are known to have low-spin triplet ground states ($S = 1$) and low-lying quintet excited states ($S = 2$) and, as such, have a more complex reactivity behavior.[7,8] The key understanding of this reactivity has been contributed by density functional theory (DFT) computations, which was characterized as the two-state reactivity (TSR),[9–11] wherein the $S = 2$ state cuts through the larger $S = 1$ barrier and modulates the reaction.[9–14] Indeed, studies on the reaction mechanism for C–H bond hydroxylation by heme and nonheme iron(IV)-oxo complexes have been extensively conducted by Que,[15] Nam,[16] Solomon,[15a] Thiel,[17] Shaik,[9,18] Siegbahn,[19] Baerends,[20] de Visser,[12,21] Neese[22] and Rajaraman *et al.*[23,24] and their respective co-workers. The C–H hydroxylation by the iron(IV)-oxo moiety is generally described as a H-abstraction/O-rebound mechanism, as proposed about 30 years ago by Groves *et al.*[25] It is well known that the activation barriers may change significantly depending on the spin multiplicity of the potential energy surfaces, and the reactants may go through more than one such surface during the reaction.[26,27] These mechanisms can be envisioned by virtue of differences in the acceptor orbitals on the reactive metal-oxo unit.

An extension to biologically relevant iron(IV)-oxo ($S = 1$) and ($S = 2$) enzyme intermediates shows that they can perform electrophilic attack reactions along the mechanistic pathway of both the π-channel with the unoccupied π*(FeO) orbital and the σ-channel involving the unoccupied α-spin Fe-σ^*_{z2} orbital. The H-atom abstraction on the quintet surface favours the σ-channel that requires a vertical approach of the cleaving C–H bond. By contrast, on the triplet surface the π-channel with an equatorial approach is the preferred one.[10,14,21,28–30] Nevertheless, Solomon *et al.* first proposed that the π-mechanism is more preferred relative to the usual σ-mechanism on the

State Key Laboratory of Theoretical and Computational Chemistry, Institute of Theoretical Chemistry, Jilin University, Changchun, People's Republic of China. E-mail: huiling@jlu.edu.cn, huangxr@jlu.edu.cn; Fax: +86 8849 8026; Tel: +86 1350440 4012

†Electronic supplementary information (ESI) available: Tables with relative energies, spin densities, and charge analysis, figures with orbital occupancy evolution diagrams, and optimized *xyz* coordinates. See DOI: 10.1039/c3dt50866h

quintet surface during the H-abstraction step in the benzylic hydroxylation of (4-hydroxy)mandelate synthase (HmaS).[31] Recent studies by Neese and co-workers on the reaction of alkane hydroxylation by ferryl model compounds not only demonstrated the existence of the triplet σ-mechanism, but also recognized that the reaction can take place through both the σ- and π-pathways on the quintet and triplet surfaces with barrier heights displaying the order $^5\sigma > {}^5\pi \approx {}^3\pi > {}^3\sigma$.[22a]

Inspired by these studies, we grew curious about whether the σ^*_{x2-y2} orbital could be viable as an electron acceptor. Thus, we recently attempted to explore all possible channels for the methane hydroxylation reaction by a series of nonheme iron(IV)-oxo complexes. Interestingly, apart from the classical ($^5\sigma$, $^3\pi$) and nonclassical ($^5\pi$) pathways reported previously, the $[Fe^{IV} = O(TMC)(SR)]^+$ (TMC = 1,4,8,11-tetramethyl-1,4,8,11-tetraazacyclotetradecane) species and its derivative $[Fe^{IV} = O(TMC)(OH)]^+$ complex were computed to involve an alternative to the H-atom abstraction mechanism in the methane C–H activation, in which the vacant σ^*_{x2-y2} orbital has been occupied on the triplet surface. This new channel is denoted hereafter as $^3\delta$-channel. To get more insight into the nature of this $^3\delta$-channel, the issues of the electron transfer process, the actual acceptor orbital, the features of the geometry, electronic property and reactivity, the factor that shapes this channel and how it compares with the other pathways should be addressed.

By answering these questions, in this paper, we have performed a DFT study of the methane hydroxylation reactions by using the $[Fe^{IV} = O(TMC)(L)]^+$ complexes, with L = SR^-, OH^-, F^-, and $CF_3CO_2^-$, and considered all possible channels on the triplet and quintet states (Scheme 1). It is worth mentioning that the $^3\pi$- and $^5\sigma$-channels mediated by **4** in the methane hydroxylation reaction have been reported in our previous work[32] by means of the same methods, procedures, and basis sets; hence, we employed the $^3\sigma$- and $^5\sigma$-channels. A full and in-depth description of the triplet δ-mechanism observed in the methane hydroxylation mediated by $[Fe^{IV} = O(TMC)(SR)]^+$ and its derivative $[Fe^{IV} = O(TMC)(OH)]^+$ complex was presented for the first time, and a systematic comparative study of their geometries, electronic properties and reactivities in hydrogen atom abstraction reactions regarding all other possibilities were investigated. Furthermore, the axial ligands effect on the reaction pathways of the iron(IV)-oxo oxidants in the methane C–H activation has also been elaborated by comparing the different channels in the reactions of CH_4 with the electron-deficient F^- and $CF_3CO_2^-$ substituents in $[Fe^{IV} = O(TMC)(L)]^+$ to those mediated by the electron-rich SR^- and OH^- ligands.

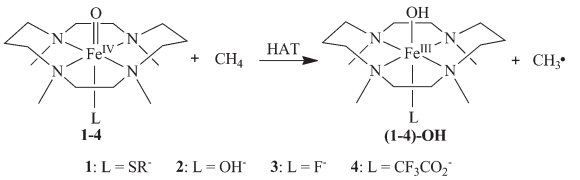

Scheme 1 The methane hydroxylation process by nonheme iron(IV)-oxo reagents with variable axial ligands: **1** ($[Fe^{IV} = O(TMC)(SR)]^+$), **2** ($[Fe^{IV} = O(TMC)(OH)]^+$), **3** ($[Fe^{IV} = O(TMC)(F)]^+$), and **4** ($[Fe^{IV} = O(TMC)(CF_3CO_2)]^+$) in this work. HAT refers to hydrogen atom transfer.

Geometric and electronic features of 1–4

All the iron(IV)-oxo complexes have two low-lying electronic states, triplet and quintet. The electron occupancies for $S = 1$ and $S = 2$ in the d-block orbitals are depicted in Fig. 1 as taken from case **1**. The same electron configurations as case **1** are observed in cases **2–4**. As inferred from Fig. 1, the doubly

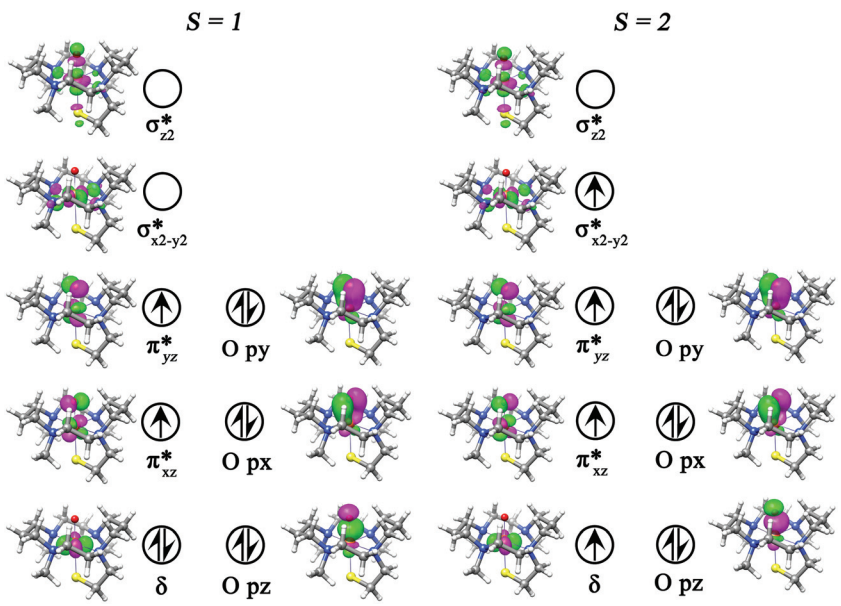

Fig. 1 Orbital occupancy diagram for the triplet ($S = 1$) and quintet ($S = 2$) states of **1**.

Table 1 Bond lengths (Å), spin densities (ρ) and Mulliken charges (Q) of **1–4** for S = 1 and S = 2 spin states in solution

	1		**2**		**3**		**4**	
	S = 1	S = 2	S = 1	S = 2	S = 1	S = 2	S = 1	S = 2
Fe–O	1.66	1.66	1.66	1.65	1.64	1.64	1.62	1.62
Fe–L	2.39	2.35	1.90	1.88	1.88	1.86	2.05	2.00
Fe–N[a]	2.14	2.23	2.14	2.23	2.12	2.21	2.14	2.23
ρFe	2.25	2.97	1.49	3.19	1.52	3.19	1.51	3.16
ρO	0.45	0.56	0.66	0.56	0.66	0.53	0.70	0.57
QFe	0.51	0.56	0.80	0.90	0.85	0.96	0.87	0.98
QO	−0.66	−0.58	−0.60	−0.57	−0.60	−0.56	−0.53	−0.49

[a] Averaged value of four Fe–N distances.

occupied δ orbital in the triplet spin state in the *xy*-plane of symmetry is orthogonal to the O–Fe–L axis, which is mostly a nonbonding orbital on the metal. Two singly occupied orbitals in the triplet spin state are the $\pi^*_{xz/yz}$ orbitals for the antibonding interactions of the metal $3d_{xz}/3d_{yz}$ orbitals with $2p_x/2p_y$ on the oxo-group. To a certain extent, the two $\pi^*_{xz/yz}$ orbitals also contain antibonding interactions with the axial ligand but to a much lesser degree than the iron-oxo interaction. The σ^*_{z2} and σ^*_{x2-y2} orbitals are virtual in the triplet spin state. The former is the σ* antibonding interactions along the O–Fe–L orientation, and the latter is the metal with the nitrogen atoms of the TMC ring, respectively. The quintet spin state differs from the triplet configuration by one-electron excitation from δ to σ^*_{x2-y2} in S = 1 to give a $(\delta)^1\ (\pi^*_{xz})^1\ (\pi^*_{yz})^1\ (\sigma^*_{x2-y2})^1$ electronic configuration.

Table 1 lists the notable geometrical parameters, spin populations and Mulliken charges computed for **1–4** in the triplet and quintet states. Focusing on the geometric details in Table 1 reveals that the Fe–O bond length does not change significantly in going from the triplet to the quintet state, since the σ^*_{x2-y2} is strongly Fe–N σ-antibonding, but both δ and σ^*_{x2-y2} orbitals are (nearly) perpendicular to the Fe–O bond. However, the equatorial ligands bind much more strongly to the iron centre in the triplet than in the quintet state (Table 1), in accordance with the occupation of the σ^*_{x2-y2} orbital, as previously found in P450 compound I[29] as well as in several nonheme iron–oxo species.[9,10,33] We note that the Fe–O bonds in **1** and **2** are longer compared to the corresponding ones in **3** and **4**, suggesting that the more electron-donating axial ligand in $[Fe^{IV} = O(TMC)(L)]^+$ makes a much stronger push effect, as reported for the thiolate ligand effect in P450.[34–36]

With regard to the relative energies of the spin states, the calculation results of B3LYP/B1, B3LYP/B2//B3LYP/B1, B3LYP-G/B2//B3LYP/B1, B3LYP + VDW/B2//B3LYP/B1, and PBE0/B2//B3LYP/B1 presented in Table S1 in the ESI† show that both **3** and **4** possess a triplet ground state at the B3LYP/B2//B3LYP/B1 level, in accord with experiment,[37] while **1** and **2** are computed to have a quintet ground state at all the functional levels in both the gas (Table S2 in ESI†) and solution (Table S1 in ESI†) phases, although **1** was experimentally found to have a triplet ground state.[38] Therefore, additional tests were performed using the B3LYP-G, B3LYP + VDW and PBE0 functionals for geometry optimizations of **1** and upgrade the energies by single-point B3LYP-G, B3LYP + VDW and PBE0 calculations on the corresponding optimized structures at the larger basis set (B2) level, respectively. However, all attempts to characterize the ground state failed. All sets of B3LYP-G/B2//B3LYP-G/B1, B3LYP + VDW/B2//B3LYP + VDW/B1, and PBE0/B2//PBE0/B1 gave generally similar results to B3LYP/B2//B3LYP/B1 with a quintet ground state (Table S3 in ESI†). Although all the functionals incorrectly predict the triplet ground state for **1** and **2**, the energy difference between the triplet and quintet states is small, especially the B3LYP and B3LYP-G results, which may be well within the error of B3LYP. This is similar to a previous study on the same oxidant,[11] which also failed to predict the correct spin state for **1**. Nevertheless, irrespective of the spin-state identity in the ground state in **1** and **2**, the main results obtained, such as the electron transfer process and the relative reactivity ordering for the respective reaction mechanism accompanying the H-abstraction reaction, have been not sufficient to be changed as indicated by the details discussed below. B3LYP and B3LYP-G results for the triplet–quintet gap were found to be smaller relative to B3LYP + VDW and PBE0. Furthermore, B3LYP/B2//B3LYP/B1 predicts the correct triplet ground states for **3** and **4**. Hence, we mainly discussed the results obtained at the B3LYP/B2//B3LYP/B1 level in this work.

Hydrogen abstraction from CH_4 by 1–4

The C–H hydroxylation reactions of methane by four different iron(IV)-oxo oxidants are investigated. As previously found,[26,27,39–41] the reaction can branch out different possible pathways in the H-atom abstraction stage, which have been studied in depth by Neese and co-workers.[22] Interestingly, in addition to the classical and nonclassical pathways, discussed above, we have observed an alternative to the H-atom abstraction mechanism (^{3}δ-channel) in the methane C–H activation by **1** and **2**. Therefore, the discussion will centre on the triplet δ-channel.

H-abstraction reaction

Fig. 2 and 3 show the hydrogen-abstraction profiles for **1** and **2**, wherein one hydrogen atom is abstracted from the reactant $^{2S+1}$**R** by ($^{2S+1}$**TS$_H$**), yielding an iron(III)-hydroxyl species

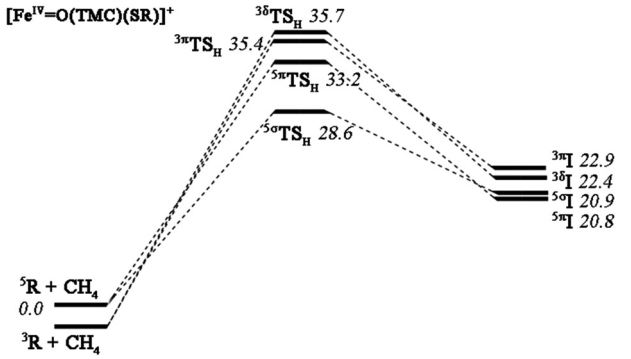

Fig. 2 Free energy profile of methane hydroxylation with **1** in acetonitrile at the B3LYP/B2//B3LYP/B1 level.

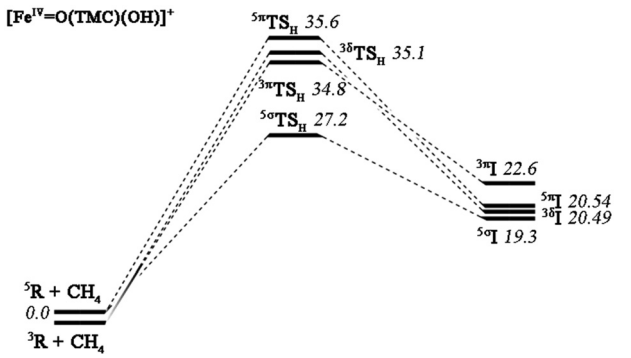

Fig. 3 Free energy profile of methane hydroxylation with **2** in acetonitrile at the B3LYP/B2//B3LYP/B1 level.

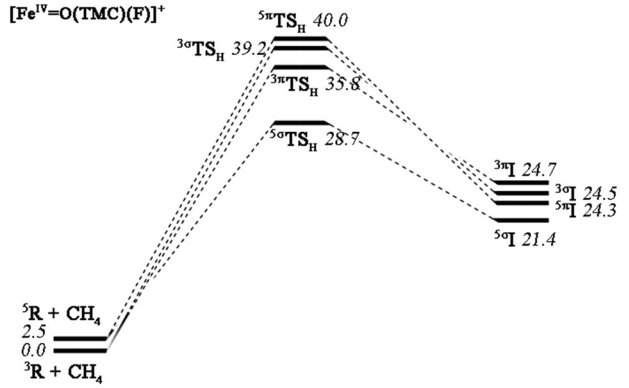

Fig. 4 Free energy profile of methane hydroxylation with **3** in acetonitrile at the B3LYP/B2//B3LYP/B1 level.

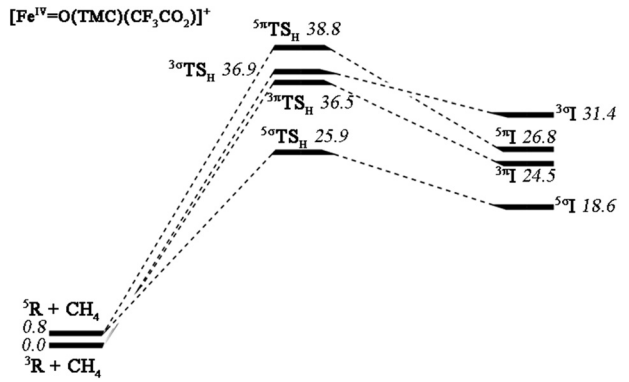

Fig. 5 Free energy profile of methane hydroxylation with **4** in acetonitrile at the B3LYP/B2//B3LYP/B1 level.

together with a carbon radical ($^{2S+1}$**IN**). We cannot expect a stable cluster in solution. The process not only proceeds through $^{3\pi}$**TS$_H$**, $^{5\pi}$**TS$_H$** and $^{5\sigma}$**TS$_H$** on the triplet and quintet surfaces, but a δ-mechanism is observed on the triplet surface as well. The free energy barriers in Fig. 2 at the B3LYP/B2//B3LYP/B1 level were 28.6, 33.2, 35.4, and 35.7 kcal mol^{-1} for ^{5}σ, ^{5}π, ^{3}π, and ^{3}δ-pathways, respectively. However, as addressed recently by Lonsdale[42] and Rajaraman *et al.*[24] and found herein too, inclusion of dispersion correction lowers the H-abstraction barriers by about 3–5 kcal mol^{-1} to 24.4, 27.8, 32.2, and 30.5 kcal mol^{-1} for ^{5}σ, ^{5}π, ^{3}π, and ^{3}δ-pathways, respectively (Table S4, ESI†). For case **2**, the free energy barriers at the B3LYP/B2//B3LYP/B1 level for $^{5\sigma}$**TS$_H$**, $^{3\pi}$**TS$_H$**, $^{3\delta}$**TS$_H$**, and $^{5\pi}$**TS$_H$** relative to the separated reactants were found to be 27.2, 34.8, 35.1, and 35.6 kcal mol^{-1}, respectively. Including the dispersion correction the barriers become 23.1, 29.9, 30.3, and 31.4 kcal mol^{-1} for ^{5}σ, ^{3}δ, ^{5}π, and ^{3}π-pathways, respectively (Table S4, ESI†). B3LYP + VDW and PBE0 yield similar trends to B3LYP for **1** and **2**, where whether the triplet **1** and **2** is an excited state or a ground state, the H-abstraction reaction is mediated by the quintet σ-pathway (^{5}σ), and the triplet π-pathway (^{3}π), the quintet π-pathway (^{5}π) and the triplet δ-pathway (^{3}δ) have comparable energy barriers (Tables S4 and S5 in the ESI†). In contrast to the mechanism in solution, the reactants of **1** and **2** in the gas-phase reactions could form a reactant cluster, followed by a transition state for hydrogen abstraction that leads to an intermediate. Otherwise, the main features of the solution-phase profile remain the same in the gas phase, such as the ordering of reaction channels, the electron transfer mechanisms. Consequently, either in the gas phase or in a low polarity medium, the relative reactivities for hydroxylation of all the nonheme iron(IV)-oxo model systems herein decrease in the order $^5\sigma > {}^5\pi \approx {}^3\delta \approx {}^3\pi$, which agrees with the previous studies,[12,19,20a,22a,40] apart from the ^{3}δ-channel discussed here.

The obtained potential energy profiles in solution are displayed in Fig. 4 and 5 when L = F$^-$ and $CF_3CO_2^-$. In both cases the H-atom abstraction reactions start from the experimentally determined S = 1 ground state, and subsequently, proceed not only through the same ^{5}σ, ^{5}π, ^{3}π-pathways as those exhibited by the oxidants **1** and **2**, but also different ^{3}σ-pathways. A TSR reactivity mechanism with crossover from the ground state triplet surface to the quintet state surface is observed for the H-atom abstraction reactions by **3** and **4**. This is consistent with previous computational studies on aliphatic hydroxylation with nonheme iron(IV)-oxo complexes, which gave preferential quintet over triplet spin mechanism.[9–12,43–46]

Electronic structure of TSHs

Now, we turn to compare the electronic structures of different pathways. Scheme 2 shows five possible electron shifts and resulting transition states, which are generated by shifting either an α or β electron to the d block for each spin state. Thus, as illustrated in Scheme 2, the d-block of $^{3\delta}$**TS$_H$** gains an electron into the vacant σ^*_{x2-y2} orbital, whereas the C–H bond orbital is converted to a single occupied orbital on the radical moiety with down spin. In contrast, $^{3\pi}$**TS$_H$** has one single spin-up electron and the other on the C radical moiety, while $^{5\pi}$**TS$_H$** has ~3 unpaired spin-up electrons in the d block and the other on the C radical moiety, as well, both of which are responsible for the π-mechanism that involves the shift of a β electron to the $\pi^*_{xz/yz}$ orbital of the iron(IV)-oxo reagent, and the formation of a C radical in the C˙ orbital. Moreover, it is seen that for both the ^{3}σ- and ^{5}σ-pathways, one α-spin electron formed in the σ_{C-H} orbital of CH_4 ends in the σ^*_{z2} orbital while the substrate orbital, C˙, retains the β-spin electron.

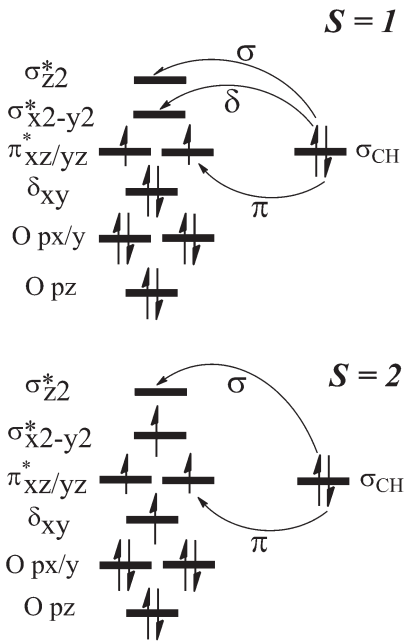

Scheme 2 Electron shifts diagrams of the possible reaction channels during H-abstraction from methane by **1–4**.

Reactivity comparison

The differential reactivity of H-atom abstraction for all the pathways can be explored next. As shown above, the ^{3}δ-channel encounters a comparable barrier to those calculated for the ^{3}π- and ^{5}π-channels due to the unavoidably increased Pauli repulsion and reduced orbital overlap compared with the ^{5}σ-pathway. Unlike $^{3\pi}$**TS$_H$**, which is not stabilized and has a higher barrier owing to the exchange depletion, the number of exchange interactions of $^{3\delta}$**TS$_H$** increases from 2 to 3 relative to the triplet reactants, by populating the σ^*_{x2-y2} orbital of the iron(IV)-oxo reagent. By contrast, in $^{5\sigma}$**TS$_H$** the d–d exchange is enhanced compared to the quintet reactants by four new interactions.[47] The greater degree of exchange stabilization in $^{5\sigma}$**TS$_H$** relative to that in $^{3\delta}$**TS$_H$** may overcome the orbital energy gap ($\sigma^*_{x2-y2} \rightarrow \sigma^*_{z2}$) and hence the barrier of $^{5\sigma}$**TS$_H$** is below that of the corresponding $^{3\delta}$**TS$_H$** species. In addition, such a similar reactivity was also found in the intermediates; that is, $^{5\sigma}$**I** is higher than $^{3\delta}$**I**.

Reaction mechanism of ^{3}δ-channel

Detailed electronic structure analysis can provide key clues for better understanding the ^{3}δ-channel. As the electronic structure in solution is similar to that in the gas phase, we mainly discuss the gas-phase ^{3}δ-mechanism on model systems **1** and **2**, and collect the analogous solution-phase results in the ESI.† Fig. 6 and 7 show the evolution of d-orbital occupancy along

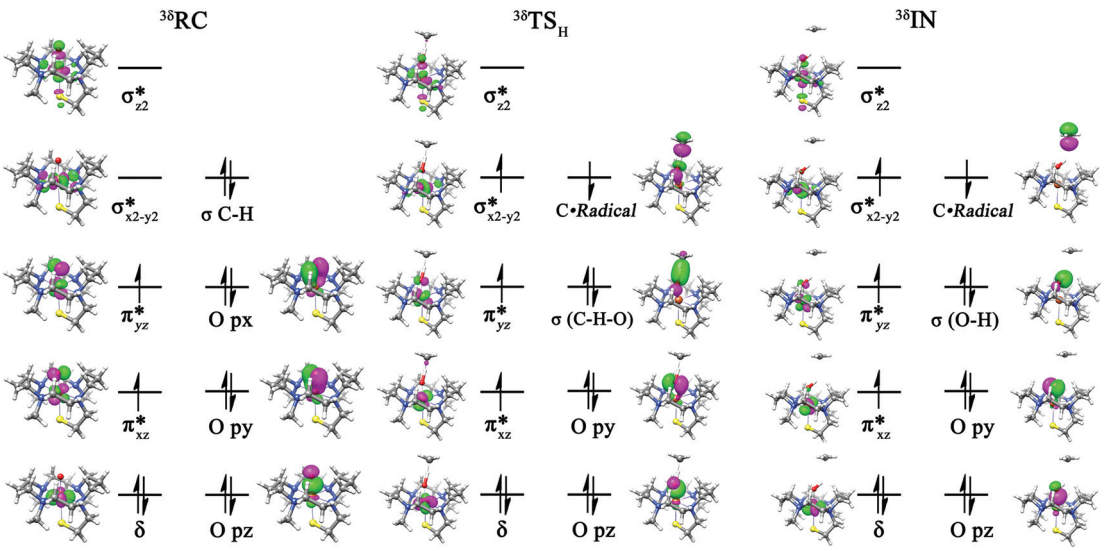

Fig. 6 Schematic MO diagrams of $^{3\delta}$**RC**, $^{3\delta}$**TS$_H$**, and $^{3\delta}$**IN** involved in the H-atom abstraction reaction for **1** with methane.

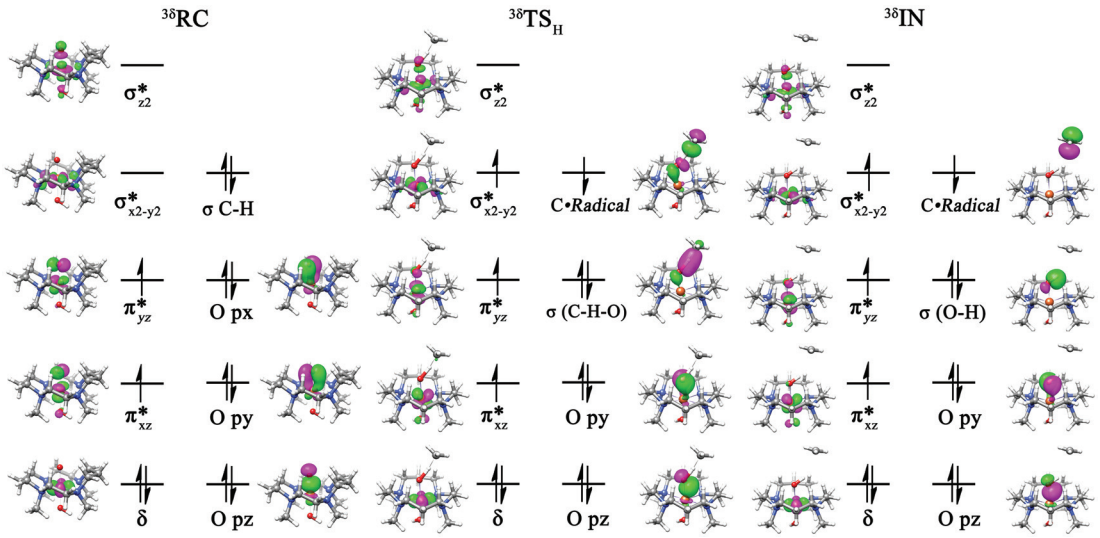

Fig. 7 Schematic MO diagrams of $^{3\delta}$**RC**, $^{3\delta}$**TS$_H$**, and $^{3\delta}$**IN** involved in the H-atom abstraction reaction for **2** with methane.

the ^{3}δ-pathway for **1** and **2** during the H-abstraction, respectively. As shown by the schematic molecular orbital diagrams in Fig. 6 and 7, the electronic structure of the reactant $^{3\delta}$**RC** is better interpreted as the Fe=O centre weakly bound to the methane substrate with a $(\delta)^2$ $(\pi^*_{xz})^1$ $(\pi^*_{yz})^1$ electronic configuration in the d-block of the iron centre. The transition state $^{3\delta}$**TS$_H$** contains a high-spin ferric ion (S_{Fe} = 3/2) that is antiferromagnetically coupled to a methyl radical (S_C = 1/2); the hydrogen-atom abstraction process through the δ-mechanism finally leads to an intermediate ($^{3\delta}$**IN**), which features antiferromagnetic coupling between an intermediate spin ferric (S_{Fe} = 3/2) and a methyl radical (S_C = 1/2). Hence, as described in Scheme 2, it is plausible to propose that one single spin-up electron flows from the σ_{C-H} orbital of CH_4 to the vacant σ^*_{x2-y2} orbital in $^{3\delta}$**TS$_H$**, leading to an iron(III)-hydroxo complex and methyl radical with the other spin-down electron of the C–H bond orbital.

A careful analysis of the group spin densities and charges collected in Tables S7 and S10 in the ESI† indicates that $^{3\delta}$**TS$_H$** has radical character with the substrate rest group ρ_{CH3} = −0.50 (−0.51) for **1** (**2**) and little charge Q_{CH3} = 0.00 (−0.01) for **1** (**2**). There is further support that $^{3\delta}$**IN** is radical in character with group spin densities of ρ_{CH3} = −0.98 (−0.97) for **1** (**2**), while the charge on this group is Q_{CH3} = 0.02 (0.03) for **1** (**2**). Therefore, the spin densities and charge analysis is consistent with the electronic structure discussed above.

Intrinsic electron acceptor orbital for the triplet δ-pathway

On the basis of the above analysis result, two possible interpretations for the triplet δ-mechanism during the H-atom abstraction process can be proposed, one of which is that one electron of the C–H bond is shifted directly to the σ^*_{x2-y2} orbital, while the other is that the $\pi^*_{xz/yz}$ orbital of the iron(IV)-oxo reagent may serve as the electron donor due to the C–H oxidation. We then inspect the intrinsic electron acceptor orbital for the triplet δ-pathway during the H-atom abstraction process. As observed in previous studies,[10,22b] direct electron transfer from the substrate to the iron centre is very unlikely, owing to the steric hindrance provided by the ligand framework, and thus the substrate can only interact with the oxo group rather than directly with the iron centre. Consequently, all possible electron transfer pathways have to pass through the O-atom, indicating that the viable electron acceptor orbitals should contain significant contributions from the O-atom in the actual H-atom abstraction. However, as the σ^*_{x2-y2} orbital is located in the plane perpendicular to the line of the substrate attack and has less significant interactions with the oxo ligand or the substrate than with the Fe d_{z2} and Fe $d_{xz/yz}$ orbitals, consequently, the electron of the C–H bond may be unlikely to directly transfer into the σ^*_{x2-y2} orbital. Then, to address the actual electron transfer process for the triplet δ-pathway, we performed a detailed electronic structure analysis of the transition state en route to the connecting reactant complexes, through a relaxed surface scan at a series of fixed values of the reaction coordinate, the O–H distance. Fig. 8 displays one of the schematic MO diagrams for **1** in the proximity of the transition state (O–H = 1.35 Å). It is apparent from the MO diagram of Fig. 8 that the methane σ_{C-H} orbital initially interacts with the O-$p_{x/y}$ based $\pi^*_{xz/yz}$-orbital. This implies that the triplet δ-mechanism may be described as the original α-spin electron transfer from the π* orbital of the catalyst to the σ^*_{x2-y2} orbital, and the α-spin electron from the σ_{C-H} orbital of the substrate shift to the just empty α-spin π* orbital of the catalyst through the O-$p_{x/y}$ based $\pi^*_{xz/yz}$-orbital concomitantly. As such, the electronic structure analysis of the TS species and of the reactant complexes en route to the transition state indicates that the final acceptor orbital for the triplet δ-pathway during the H-atom abstraction process is the α-spin σ^*_{x2-y2} orbital. By contrast, on the π-pathway the acceptor orbital is the β-spin O-$p_{x/y}$ based $\pi^*_{xz/yz}$-orbital, while the α-spin O-p_z based σ^*_{z2}-orbital is the acceptor orbital for the σ-mechanism, which agrees with the previous studies.[22,40,41]

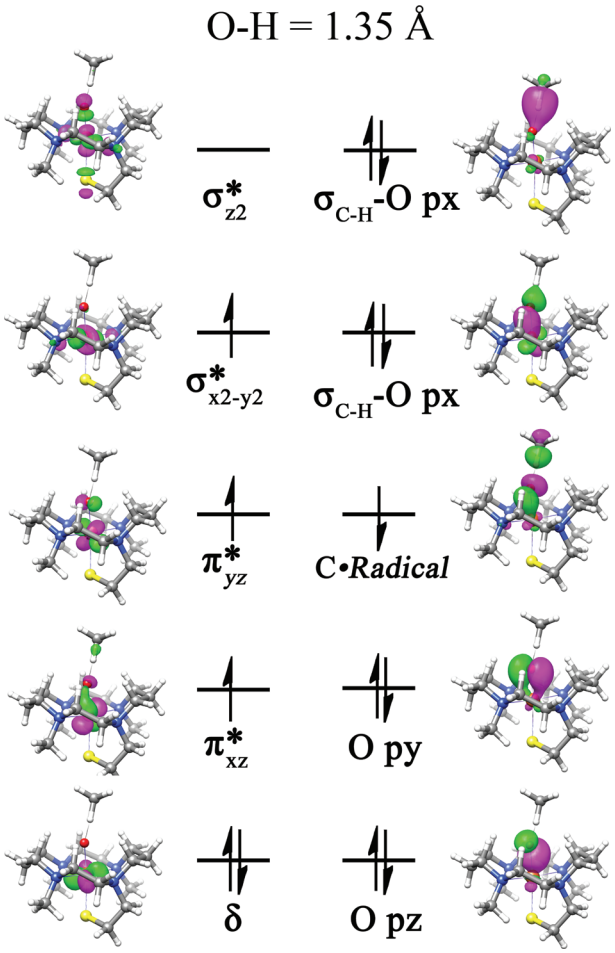

Fig. 8 Schematic MO diagram illustrating the evolution of the key MO of $^{3\delta}$**RC** en route to $^{3\delta}$**TS$_H$** involved in the H-atom abstraction reaction for **1** with methane.

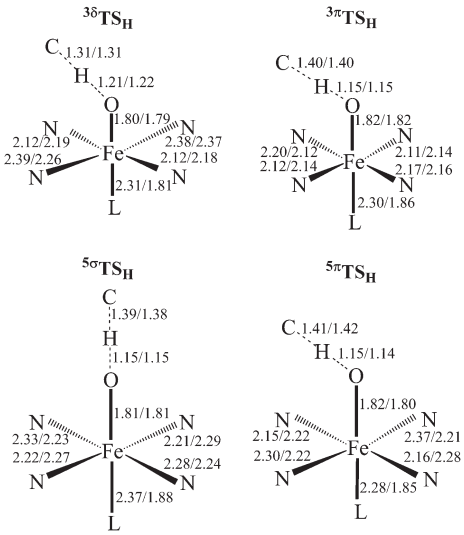

Fig. 9 Comparison of the key structural features of $^{3\delta}$**TS$_H$**, $^{3\pi}$**TS$_H$**, $^{5\sigma}$**TS$_H$** and $^{5\pi}$**TS$_H$** for **1**/**2** reacting with methane in the gas phase. Bond lengths are in Ångstroms, and angles are in degrees.

Geometric structures of TSHs

The detailed geometric structures of the transition states in the gas and solution phases for C–H cleavage are displayed in Fig. 9 and 10. The different reaction mechanisms also define structural selection rules for the corresponding transition states. As can be seen from Fig. 9 and 10, the $^{3\delta}$**TS$_H$** in the ^{3}δ-mechanism has a distorted octahedral structure, where the metal ion is surrounded by two shorter bonds opposite each other (*trans*), and two significantly elongated bonds in the *xy* plane. Apparently, this key geometry feature coincides well with the ^{3}δ-mechanism in which the σ^*_{x2-y2} orbital serves as the electron acceptor: first, the two shorter bonds of Fe–O and Fe–L can make the antibonding character more strengthened and increase the energy of the σ^*_{z2} orbital of the complex, thus enhancing the probability of occupancy of the vacant σ^*_{x2-y2} orbital in the triplet state. Second, the two obviously elongated equatorially and diagonally Fe–N bonds may weaken the σ interaction between the σ^*_{x2-y2} orbital and the equatorial ligands, making the energy of the σ^*_{x2-y2} orbital lower, and hence provides a chance for the occupied σ^*_{x2-y2} orbital. Such geometric characteristics of the triplet δ-pathway are further tried to be comprehended from the viewpoint of the Jahn–Teller effect, which has an important role to play in stabilizing different pathways and to preferentially select a particular mechanism. Note that the d_{x2-y2} being orthogonal to the oxygen p-orbital is not the only possibility at $S = 2$ (or other spin-states) but is likely to be the global minimum with other Jahn–Teller isomers being closer (much closer than the energy estimate of different pathways). As the ligands move further out, the splitting of the octahedral levels increases. Again, the effect is more marked for the d_{z2} and d_{x2-y2} orbitals because they are directed towards the ligands. Now let us consider the situation of the triplet δ-pathway in which the two *trans* ligands are moved closer to the iron ion, and the two in the *xy* plane are moved further out. In this case, the *trans* ligands will repel an electron in the d_{z2} orbital more than they would in a regular octahedral complex, leading to the even higher energy of the d_{z2} orbital relative to that in the regular octahedral complex. Thus, the two e_g orbitals in the octahedral complex are no longer at the same level of energy; that is, their energy degeneracy has been lifted, and the energy of the d_{x2-y2} orbital will be lower regarding the d_{z2} orbital. Meanwhile, the original t_{2g} level will also split into e_g (d_{xz}, d_{yz}) at the higher level and d_{xy} at the lower level. Inspecting the O–H bond and the C–H bond in Fig. 9 and 10 reveals that the $^{3\delta}$**TS$_H$** is an early transition state as suggested by a longer O–H bond and a shorter C–H bond identified in $^{3\delta}$**TS$_H$** relative to those in $^{3\pi}$**TS$_H$**, $^{5\pi}$**TS$_H$**, and $^{5\sigma}$**TS$_H$**. Another key feature is reflected by the Fe–O–H angles in the different pathways at the respective transition states. The gas-phase Fe–O–H angles of 141.2° and 137.2° in $^{3\delta}$**TS$_H$** for **1** and **2** closely resemble what was found in the π-mechanisms (138.4° and 137.1° in $^{3\pi}$**TS$_H$** and 138.1° and 136.5° in $^{5\pi}$**TS$_H$** for **1** and **2**). So did the Fe–O–H angles calculated in solution (Fig. 10). This can be rationalized with regard

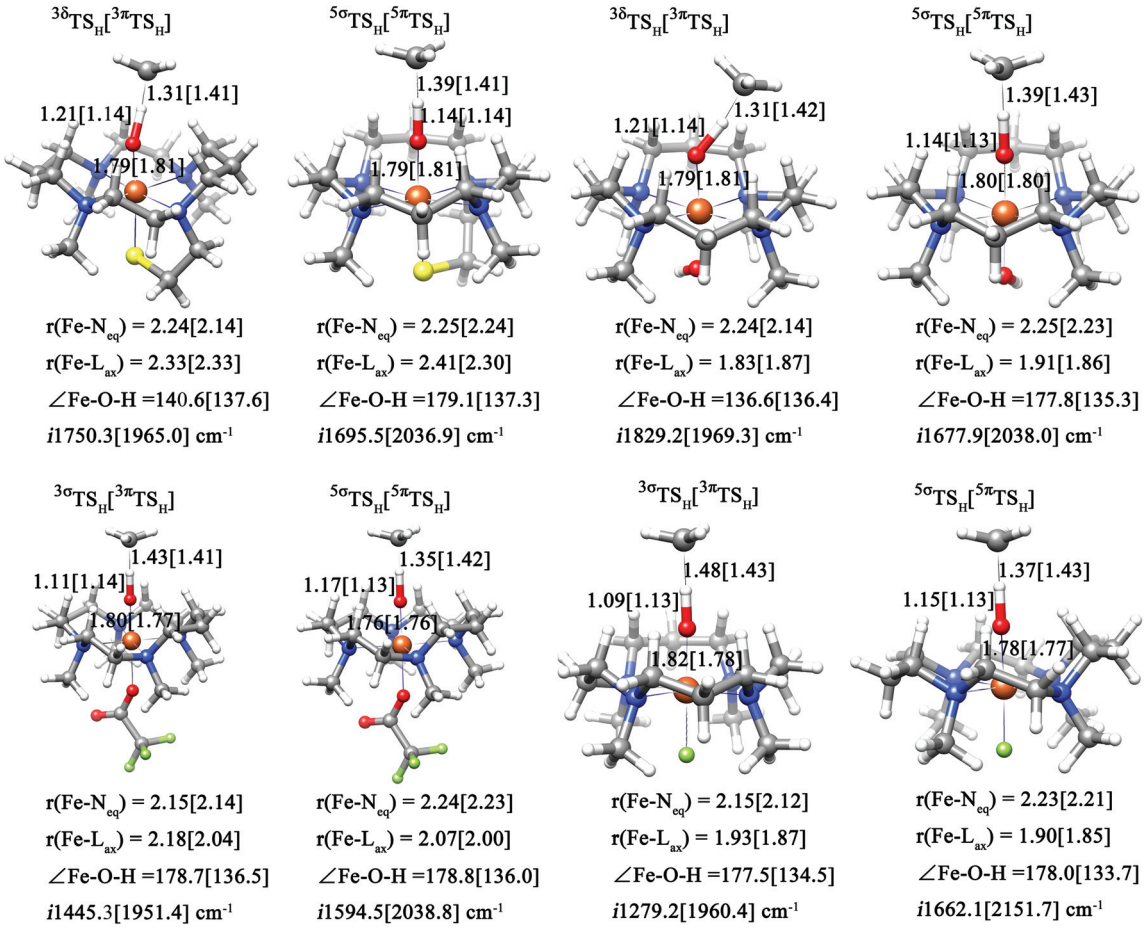

Fig. 10 Geometric details of hydrogen-abstraction transition states of **1–4** for the triplet and quintet spin states in acetonitrile. Bond lengths are in Ångstroms, angles are in degrees and the imaginary frequency in the transition state is in wave numbers.

to the electron transfer on both the triplet δ and π-pathways from the substrate to the final electron acceptors of Fe centre by means of the same O-$p_{x/y}$ based $\pi^*_{xz/yz}$-orbital, despite different donor and final acceptor orbitals. A sideways trajectory with an Fe–O–H angle close to 120° for δ and π-mechanisms results from the compromise between the orbital interaction and the Pauli repulsion.[22b] However, the Fe–O–H angles of approximately 180° in $^{3,5\sigma}\mathbf{TS_H}$ for **1–4** can thus be attributed to the occupancy of the σ^*_{z2} orbital[9–11,15a,20c,28] in the σ-pathway, which features significantly smaller Pauli repulsion and better orbital overlap in comparison with the δ and π-pathways.

The axial ligand effect on the reaction channels

Interestingly, in addition to the ^{3}π-, ^{5}π- and ^{5}σ-channels, the ^{3}δ-channel was found in the H-abstraction reaction mediated by the stronger electron-donating SR^- and OH^- substituents in $[Fe^{IV}=O(TMC)(L)]^+$, while the C–H activation mediated by the weaker electron-donating F^- and $CF_3CO_2^-$ substituents proceeded *via* the ^{3}σ-channel rather than the ^{3}δ-channel. The difference in the behaviours of **1**, **2** and **3**, **4** is ascribed to differences in the electron-donating ability of the axial ligand. This may arise mainly from the degree of the destabilization effect of the σ^*_{z2} orbital by the strong and weak donating ligands. Clearly, when the axial ligand is a good electron donor like SR^- and OH^-, the σ^*_{z2} orbital has been dramatically destabilized, leading to strong Fe–L antibonding character[10,11,15a,20b,47–50] and too high in the energy of the σ^*_{z2} orbital to come into play in the σ-pathway. Therefore, it is easier for the electron to transfer to the σ^*_{x2-y2} orbital than to the σ^*_{z2} orbital during S = 1. In contrast, the weak donors like F^- and $CF_3CO_2^-$ make the σ^*_{z2} orbital more favourable relative to the strong donors. Consequently, based on the above analysis one may anticipate that the axial ligand can modulate the reaction pathways *via* varying the electron pushing abilities of the axial ligands with regard to H-atom abstraction toward methane for the iron-oxo complexes described herein.

Conclusion

All the possible channels for the methane hydroxylation reaction by the $[Fe^{IV}=O(TMC)(L)]^+$ complex (L = SR^-, OH^-, F^-, and

$CF_3CO_2^-$) have been theoretically investigated on the triplet and quintet states. We have described for the first time the δ-mechanism on the triplet surface in the H-abstraction reaction mediated by $[Fe^{IV} = O(TMC)(SR)]^+$ and its derivative $[Fe^{IV} = O(TMC)(OH)]^+$ complex. Furthermore, this work gave detailed insight into the nature of this pathway and how it compares with all other possibilities, including relative reactivities, geometries, energetic and electronic structural features. Insights into the electron transfer process accompanying the H-abstraction reaction for the triplet δ-mechanism are achieved through a detailed electronic structure analysis of the transition state species and the reactant complexes en route to the transition state. It is found that the electron transfer from the σ_{C-H} orbital of the substrate into the final acceptor σ^*_{x2-y2} orbital of the catalyst occurs through a complex mechanism that is initiated by the original α-spin electron transfer from the π* orbital of the catalyst to the σ^*_{x2-y2} orbital, where the α-spin electron from the σ_{C-H} orbital of the substrate shift to the just empty α-spin π* orbital of the catalyst *via* the O-$p_{x/y}$ based $\pi^*_{xz/yz}$-orbital concomitantly. The reactivity of the ^{3}δ-pathway is comparable with the ^{3}π- and ^{5}π-pathways, while the ^{5}σ-channel is energetically more favourable than the ^{3}δ-pathway by exchange stabilization.[29,47–50] Additionally, the axial ligand can modulate the reaction pathways *via* varying the electron pushing abilities of the axial ligands with regard to H-atom abstraction toward methane for the iron(IV)-oxo complexes as indicated by the observation that the ^{3}δ-channel was found in the H-abstraction reaction mediated by the stronger electron-donating SR^- and OH^- substituents in $[Fe^{IV} = O(TMC)(L)]^+$, while the C–H activation mediated by the weaker electron-donating F^- and $CF_3CO_2^-$ substituents proceeded by the ^{3}σ-channel rather than the ^{3}δ-channel. Thus, this thorough mechanistic understanding of the ^{3}δ-channel, especially the electronic structure analysis, can provide crucial insights into the H-atom abstraction reaction and further complement the experimental information. It is highly anticipated that the upcoming endeavours on elaborating the factors stabilizing the δ-type mechanism over the other quintet and triplet mechanisms as well as exploring potential systems that can feature such a scenario would hold valuable promise for this area of research.

Computational details

Density functional theory (DFT) calculations were performed with the ORCA program package.[51] For geometry optimizations, we used the hybrid B3LYP density functional[52,53] in combination with the def2-TZVP basis sets[54] on the active atoms Fe, O, C and the transferred H atom as well as the triple-ζ quality TZVP basis sets[55] on the remaining atoms. The RIJCOSX approximation[56] was used to accelerate the calculations in combination with the auxiliary basis sets def2-TZV/J (the active atoms Fe, O, C and the transferred H atom) and TZV/J (rest).[57–59] This kind of basis set system is labelled as B1. The geometries of **1** and **2** were optimized in the gas phase at the B3LYP/B1 level. For **1**, **2**, **3**, and **4**, the solvent effects were also tested through geometry optimization (B3LYP/B1 level) using the conductor like screen model (COSMO), and acetonitrile was chosen as the solvent. In order to find out which functional is suitable for predicting the spin state of **1**, we have tested many functionals. Reaction pathways were verified by scan calculations along given values of the reaction coordinate. The geometry at the top of the energy scan was used for subsequent optimization of a transition state. Geometry optimizations were fully performed without symmetry constraints. Harmonic vibrational frequencies verified that the minimum structures reported in this paper show only positive eigenvalues of the Hessian matrix and that the transition states (TSs) have only one negative eigenvalue. The zero-point energies, thermal corrections and entropy terms for the optimized geometries were obtained from these frequency calculations. Subsequent single point calculations were also performed with the hybrid B3LYP density functional using the new default basis sets of triple-ζ quality including high angular momentum polarization functions (def2-TZVPP)[60] for all elements. The density fitting and chain of spheres (RIJCOSX) approximations have been employed together with the def2-TZVPP/J auxiliary basis set,[61] labelled as B2. B3LYP with dispersion correction (B3LYP + VDW)[24,62] and B3LYP-G, and PBE0 functionals[63] were used in single-point calculations on B3LYP-optimized structures at the larger basis set (B2) level. All the results are tabulated in the ESI.†

Acknowledgements

This work was supported by the National Basic Research Program of China (973 Program) (2012CB932800), the National Natural Science Foundation of China (NSFC No. 21073075 and 21173097), the Research Fund for the Doctoral Program of Higher Education of China (RFDP No. 20100061110046), and the Fundamental Research Fund of Jilin University (No. 201003043).

Notes and references

1 E. I. Solomon, T. C. Brunold, M. I. Davis, J. N. Kemsley, S. K. Lee, N. Lehnert, F. Neese, A. J. Skulan, Y. S. Yang and J. Zhou, *Chem. Rev.*, 2000, **100**, 235–349.
2 C. Krebs, D. G. Fujimori, C. T. Walsh and J. M. Bollinger Jr., *Acc. Chem. Res.*, 2007, **40**, 484–492.
3 M. Costas, M. P. Mehn, M. P. Jensen and L. Que Jr., *Chem. Rev.*, 2004, **104**, 939–986.
4 I. Schlichting, J. Berendzen, K. Chu, A. M. Stock, S. A. Maves, D. E. Benson, R. M. Sweet, D. Ringe, G. A. Petsko and S. G. Sligar, *Science*, 2000, **287**, 1615–1622.
5 T. Spolitak, J. H. Dawson and D. P. Ballou, *J. Biol. Chem.*, 2005, **280**, 20300–20309.
6 W. Nam, *Acc. Chem. Res.*, 2007, **40**, 522–531.
7 L. Que Jr., *Acc. Chem. Res.*, 2007, **40**, 493–500.

8 L. Que Jr., *J. Inorg. Biochem.*, 2006, **100**, 421–433.
9 D. Kumar, H. Hirao, L. Que Jr. and S. Shaik, *J. Am. Chem. Soc.*, 2005, **127**, 8026–8027.
10 H. Hirao, D. Kumar, L. Que Jr. and S. Shaik, *J. Am. Chem. Soc.*, 2006, **128**, 8590–8606.
11 H. Hirao, L. Que Jr., W. Nam and S. Shaik, *Chem.–Eur. J.*, 2008, **14**, 1740–1756.
12 S. P. de Visser, *J. Am. Chem. Soc.*, 2006, **128**, 9813–9824.
13 A. J. Johansson, M. R. Blomberg and P. E. M. Siegbahn, *J. Phys. Chem. C*, 2007, **111**, 12397–12406.
14 L. Bernasconi, M. L. Louwerse and E. J. Baerends, *Eur. J. Inorg. Chem.*, 2007, **40**, 3023–3033.
15 (*a*) A. Decker, J. Rohde, E. J. Klinker, S. D. Wong, L. Que Jr. and E. I. Solomon, *J. Am. Chem. Soc.*, 2007, **129**, 15983–15996; (*b*) F. Li, K. K. Meier, M. A. Cranswick, M. Chakrabarti, K. M. Van Heuvelen, E. Münck and L. Que Jr., *J. Am. Chem. Soc.*, 2011, **133**, 7256–7259; (*c*) H. Hirao, F. Li, L. Que Jr. and K. Morokuma, *Inorg. Chem.*, 2011, **50**, 6637–6648.
16 (*a*) M. S. Seo, N. H. Kim, K.-B. Cho, J. E. So, S. K. Park, M. Clemancey, R. Garcia-Serres, J.-M. Latour, S. Shaik and W. Nam, *Chem. Sci.*, 2011, **2**, 1039–1045; (*b*) W. Nam, *Acc. Chem. Res.*, 2007, **40**, 465–465; (*c*) K.-B. Cho, H. Chen, D. Janardanan, S. P. de Visser, S. Shaik and W. Nam, *Chem. Commun.*, 2012, **48**, 2189–2191.
17 J. C. Schöneboom, S. Cohen, H. Lin, S. Shaik and W. Thiel, *J. Am. Chem. Soc.*, 2004, **126**, 4017–4034.
18 S. Shaik, D. Kumar and S. P. de Visser, *J. Am. Chem. Soc.*, 2008, **130**, 10128–10140.
19 P. E. M. Siegbahn and T. Borowski, *Acc. Chem. Res.*, 2006, **39**, 729–738.
20 (*a*) B. Ensing, F. Buda, M. C. M. Gribnau and E. J. Baerends, *J. Am. Chem. Soc.*, 2004, **126**, 4355–4365; (*b*) C. Michel and E. J. Baerends, *Inorg. Chem.*, 2009, **48**, 3628–3638; (*c*) L. Bernasconi and E. J. Baerends, *Eur. J. Inorg. Chem.*, 2008, **10**, 1672–1681.
21 S. P. de Visser, *J. Am. Chem. Soc.*, 2006, **128**, 15809–15818.
22 (*a*) C. Y. Geng, S. F. Ye and F. Neese, *Angew. Chem., Int. Ed.*, 2010, **49**, 5717–5720; (*b*) S. F. Ye and F. Neese, *Proc. Natl. Acad. Sci. U. S. A.*, 2011, **108**, 1228–1233.
23 M. Jaccob and G. Rajaraman, *Dalton Trans.*, 2012, **41**, 10430–10439.
24 A. Ansari, A. Kaushik and G. Rajaraman, *J. Am. Chem. Soc.*, 2013, **135**, 4235–4249.
25 J. T. Groves and G. A. McClusky, *J. Am. Chem. Soc.*, 1976, **98**, 859–861.
26 S. Shaik, D. Kumar, S. P. de Visser, A. Altun and W. Thiel, *Chem. Rev.*, 2005, **105**, 2279–2328.
27 S. Shaik, H. Hirao and D. Kumar, *Acc. Chem. Res.*, 2007, **40**, 532–542.
28 S. F. Ye and F. Neese, *Curr. Opin. Chem. Biol.*, 2009, **13**, 89–98.
29 H. Hirao, D. Kumar, W. Thiel and S. Shaik, *J. Am. Chem. Soc.*, 2005, **127**, 13007–13018.
30 J. Rossmeisl, K. Dimitrievski, P. Siegbahn and J. K. Norskov, *J. Phys. Chem. C*, 2007, **111**, 18821–18823.
31 M. L. Neidig, A. Decker, O. W. Choroba, F. Huang, M. Kavana, G. R. Moran, J. B. Spencer and E. I. Solomon, *Proc. Natl. Acad. Sci. U. S. A.*, 2006, **103**, 12966–12973.
32 H. Tang, G. Gia, H. L. Liu and X. R. Huang, *Inorg. Chem.*, 2013, **52**, 2684–2689.
33 F. Neese, *J. Inorg. Biochem.*, 2006, **100**, 716–726.
34 M. Sono, M. P. Roach, E. D. Coulter and J. H. Dawson, *Chem. Rev.*, 1996, **96**, 2841–2887.
35 T. Spolitak, J. H. Dawson and D. P. Ballou, *J. Biol. Chem.*, 2005, **280**, 20300–20309.
36 I. G. Denisov, T. M. Makris and S. G. Sligar, *J. Biol. Chem.*, 2001, **16**, 11648–11652.
37 J.-U. Rohde and L. Que Jr., *Angew. Chem., Int. Ed.*, 2005, **44**, 2255–2258.
38 M. R. Bukowski, K. D. Koehntop, A. Stubna, E. L. Bominaar, J. A. Halfen, E. Münck, W. Nam and L. Que Jr., *Science*, 2005, **310**, 1000–1002.
39 H. Tang, G. Gia, H. L. Liu and X. R. Huang, *Phys. Chem. Chem. Phys.*, 2012, **14**, 12863–12874.
40 D. Janardanan, D. Usharani, H. Chen and S. Shaik, *J. Phys. Chem. Lett.*, 2011, **2**, 2610–2617.
41 A. Rosa and G. Ricciardi, *Inorg. Chem.*, 2012, **51**, 9833–9845.
42 R. Lonsdale, J. N. Harvey and A. J. Mulholland, *J. Phys. Chem. Lett.*, 2010, **1**, 3232–3237.
43 S. P. de Visser and W. Nam, *J. Phys. Chem. A*, 2008, **112**, 12887–12895.
44 S. P. de Visser, *Angew. Chem.*, 2006, **118**, 1822–1825, (*Angew. Chem., Int. Ed.*, 2006, **45**, 1790–1793).
45 J. Bautz, P. Comba, C. Lopez de Laorden, M. Menzel and G. Rajaraman, *Angew. Chem.*, 2007, **119**, 8213–8216, (*Angew. Chem., Int. Ed.*, 2007, **46**, 8067–8070).
46 P. Comba, M. Maurer and P. Vadivelu, *Inorg. Chem.*, 2009, **48**, 10389–10396.
47 D. Janardanan, Y. Wang, P. Schyman, L. Que Jr. and S. Shaik, *Angew. Chem., Int. Ed.*, 2010, **49**, 3342–3345.
48 H. Chen, W. Z. Lai and S. Shaik, *J. Phys. Chem. Lett.*, 2010, **1**, 1533–1540.
49 S. Shaik, H. Chen and D. Janardanan, *Nature Chem.*, 2011, **3**, 19–27.
50 K. B. Cho, S. Shaik and W. Nam, *Chem. Commun.*, 2010, **46**, 4511–4513.
51 F. Neese, *ORCA – An ab initio, Density Functional and Semi-empirical Program Package Version 2.8*, University Bonn, Bonn (Germany), 2010.
52 A. D. Becke, *J. Chem. Phys.*, 1993, **98**, 5648–5652.
53 C. T. Lee, W. T. Yang and R. G. Parr, *Phys. Rev. B: Condens. Matter*, 1988, **37**, 785–789.
54 F. Weigend and R. Ahlrichs, *Phys. Chem. Chem. Phys.*, 2005, **7**, 3297–3305.
55 A. Schäfer, C. Huber and R. Ahlrichs, *J. Chem. Phys.*, 1994, **100**, 5829–5835.
56 F. Neese, F. Wennmohs, A. Hansen and U. Becker, *Chem. Phys.*, 2009, **356**, 98–109.

57 K. Eichkorn, O. Treutler, H. Ohm, M. Häser and R. Ahlrichs, *Chem. Phys. Lett.*, 1995, **240**, 283–290.
58 K. Eichkorn, F. Weigend, O. Treutler and R. Ahlrichs, *Theor. Chem. Acc.*, 1997, **97**, 119–124.
59 K. Eichkorn, O. Treutler, H. Ohm, M. Häser and R. Ahlrichs, *Chem. Phys. Lett.*, 1995, **242**, 652–660.
60 F. Weigend and R. Ahlrichs, *Phys. Chem. Chem. Phys.*, 2005, **7**, 3297–3305.
61 F. Weigend, *Phys. Chem. Chem. Phys.*, 2006, **8**, 1057–1065.
62 (*a*) S. Grimme, J. Antony, S. Ehrlich and H. Krieg, *J. Chem. Phys.*, 2010, **132**, 154104; (*b*) S. Grimme, *J. Comput. Chem.*, 2004, **25**, 1463–1473; (*c*) S. Grimme, *J. Comput. Chem.*, 2006, **27**, 1787–1799.
63 C. Adamo and V. Barone, *J. Chem. Phys.*, 1999, **110**, 6158–6170.